Data-driven Modeling Implementation within Materials Development and Manufacturing Systems

Allen Jonathan Román

A dissertation submitted in partial fulfillment of

the requirements for the degree of

Doctor of Philosophy

(Mechanical Engineering)

at the

UNIVERSITY OF WISCONSIN-MADISON

2023

Date of final oral examination: September 14th, 2023

The dissertation is approved by the following members of the Final Oral Examination Committee:

Tim A. Osswald, Professor, Mechanical Engineering
Lih-Sheng Turng, Professor, Mechanical Engineering
Pavana Prabhakar, Assistant Professor, Civil and Environmental Engineering
Alejandro Roldán-Alzate, Assistant Professor, Mechanical Engineering
Lianyi Chen, Assistant Professor, Mechanical Engineering

Abstract

Predicting polymeric material behavior during processing and predicting final part properties continues to be a strong research focus within the scientific community as it involves taking into consideration a wide range of time-dependent variables. By use of data-driven modeling, the materials development process can be accelerated, and the highly predictive modeling techniques can facilitate the development of smart manufacturing systems.

This dissertation worked on solving polymer engineering problems by use of data-driven modeling techniques. The first strategy was using data-driven modeling to provide a predictive model with statistical insights of the injection molding process to ensure part quality is maximized for a highly viscoelastic material blend. By injection molding highly viscoelastic materials, the probability of part defects is increased, therefore, it was crucial to use advanced computational techniques to understand the nuances of this highly non-linear process and to predict the outcome before creating material waste from faulty trials.

The second strategy was in the use of data-driven modeling for reverse engineering purposes, specifically within materials development. By combining experimental characterization and data-driven modeling, algorithms were developed and compared to prove how highly predictive models can be used as reverse engineering toolboxes. This ultimately informed users of the optimal formulation which would reach the specified target material properties.

The final strategy explored using data-driven modeling to validate the high influence of viscous heating within the pressure melt removal process, therefore, work was done in implementing a viscous heating system within a fused filament fabrication (FFF) 3D printer to accelerate the 3D printing process. The instrumented FFF 3D printer proved capable of accelerating print speeds and improving mechanical performance of 3D printed parts, working towards solving two of the largest bottlenecks within additive manufacturing: lead times and part quality. Given the unique capabilities of the data-driven modeling, the novel 3D printer was tested and evaluated via data-driven modeling to provide statistical information regarding which processing parameters were the most influential for improving overall performance of the 3D printing system.

The results of this work provide a basis for future research endeavors related to combining data-driven modeling and polymer science, such as in optimizing the newly developed viscous heating 3D printer.

Keywords: Data-driven Modeling, Polymer processing, Materials Development, FFF

Acknowledgements

First, I'd like to thank my advisor and mentor, Professor Tim Osswald as he provided me with an amazing opportunity to grow alongside many great researchers at the Polymer Engineering Center. You have provided me with countless technical support and numerous jokes to include within my repertoire. *Seguiré poniendo en alto a los Latinos y mi 0.7% parte judía.*

My deepest gratitude to the members of my dissertation committee: Prof. Turng, Prof. Prabhakar, Prof. Roldán and Prof. Chen. Thank you for your valuable input, time, and support throughout my time as a graduate student.

I also would like to show my gratitude to all of the undergraduate students, professionals and visiting scholars who made this research possible. Special mentions go to Juan Blanco, John Estela, Tzu-Chuan Chang, Abrahan Bechara, Oliyad Dibisa, and Shiyi Qin, whose brainstorming sessions represent an integral part in my growth as a researcher. Of course, I must thank the PEC family as the PEC was much more than a research lab. The PEC embodied a home away from home as we all struggled together and celebrated together our personal and professional successes.

It is also important to thank Diana, my fiancé, whose unwavering support helped me stay afloat throughout my PhD and is the reason why I am writing this dissertation. Thanks to Elsie, my sister, you and Diana inspired me to be involved in my community and to pursue goals bigger than myself.

Lastly, Mom and Dad, you walked for days across a desert to give Elsie and me the opportunity to pursue our dreams. You sacrificed everything for us, taught us the most valuable life-lessons and are my inspiration. *Les debo todo a ustedes y espero un día ser grandioso como ustedes.*

Front Matter

Abstract i
Acknowledgements ii
Symbols and Acronyms v
List of Figures ix
List of Tables xiii

Introduction 1

1. Background 3

1.1 Modeling Approaches 3
1.2 Best Practices for Data-Driven Algorithm Development 4
1.3 Linear and Logistics Regression. 5
1.4 Response Surface Methodology 6
1.5 Support Vector Machine (SVM) 9
1.6 Artificial Neural Networks (ANN) 11
1.7 Gaussian Process Regression (GPR) 12
1.8 Progress in Data-Driven Modeling within Polymer Science. 13

2. Manufacturing Process Outcome Prediction via Machine Learning 15

2.1 Introduction. 15
2.2 Materials and characterization methods 17
2.3 Methodology. 18
2.4 Results and discussion 21

3. Materials Development Optimization via Data-Driven Modeling 34

3.1 Introduction 34

3.2 Materials and characterization methods. 36

3.3 Computational methods 41

3.4 Characterization results and discussion 43

3.5 Computational results 51

3.6 Materials design optimization. 57

4. Viscous Heating Fused Filament Fabrication 3D Printer 61

4.1 Motivation for Optimizing Fused Filament Fabrication 3D Printing. 61

4.2 Introduction of Viscous Heating 63

4.2.1. Proof of Concept Experimental Setup. 64

4.2.2. Influence of Viscous Heating to Melt Throughput. 67

4.2.3. Statistical Analysis of Viscous Heating 71

4.3 Rotating Nozzle Fused Filament Fabrication 3D Printer 73

4.3.1 General Construction of 3D Printer 73

4.3.2. Influence of Rotating Nozzle on Print Forces 76

4.3.3. Influence of Rotating Nozzle on Microstructure 82

4.4 Mechanical Performance of 3D Printed Components 94

4.4.1 Influence of Rotating Nozzle on Ultimate Tensile Strength. 96

5. Summary 101

5.1 Contributions. 101

5.2. Recommendations for Future Work 102

5.3 Research Products. 105

Bibliography 110

List of Acronyms

1-D	One-dimensional
2-D	Two-dimensional
3-D	Three-dimensional
AM	Additive Manufacturing
ANN	Artificial Neural Network
BO	Bayesian Optimization
CAE	Computer aided engineering
CB	Carbon Black
CNC	Computer Numerical Control
CV	Cross-validation
DA	Dimensional Analysis
DMA	Dynamic Mechanical Analyzer
DOE	Design of experiment
DSC	Differential Scanning Calorimetry
FDM	Fused Deposition Modeling
FEA	Finite Element Analysis
FFF	Fused Filament Fabrication
FL	Fiber length
FO	Fiber orientation
GPR	Gaussian Process Regression
HA	Shore A hardness
HDPE	High-density Polyethylene
iARD-RPR	Improved Anisotropic Rotary Diffusion with the Retarding Principal Rate model
LAOS	Large Amplitude Oscillatory Strain
LR	Linear Regression
LR	Logistics Regression
MAE	Mean Absolute Error
MFI	Melt Flow Index
ML	Machine Learning
MPa	Megapascal
MW	Molecular Weight
NN	Neural Network
NR	Natural Rubber
PA	Nylon

PA66	Nylon 66
PEC	Polymer Engineering Center
PEEK	Polyether ether ketone
PP	Polypropylene
PPH	Part per Hundred
PTFE	Polytetrafluoroethylene
RBF	Radial Basis Kernel
RPM	Revolution per Minute
RSM	Response Surface Method
SABIC	Saudi Basic Industries Corporation
SVM	Support Vector Machine
TMTD	Tetrmethylthiuram Disulfide
TTS	Time Temperature Superposition
UHMW	Ultra-high Molecular Weight
VH	Viscous Heating
ZnO	Zinc Oxide

List of Symbols

a_{11}	Fiber orientation tensor in the flow direction
a_{22}	Fiber orientation tensor in the crossflow direction
a_{33}	Fiber orientation in the thickness direction
b	SVM Bias
β_0	Linear/Logistics regression intercept
β_i	Linear/Logistics regression feature weights
C_m	Fiber-matrix interaction coefficient
C_i	Fiber-Fiber interaction coefficient
De	Deborah Number
ε	Linear/Logistics regression computed error
F_{sz}	Filament Force
F	Force
h	Hours
Hz	Hertz
l	Length of Part
L_N	Number Average Fiber Length
L_W	Weight Average Fiber Length
N_i	Number of Fiber
K	Fiber Breakage Coefficient
R^2	R-squared
$R^2_{adjusted}$	R-squared of the variation in the response
$R^2_{predictions}$	R-squared of predictions
x_i	SVM feature variable
w_i	SVM feature weight
λ	Relaxation time
T_g	Glass transition temperature
μ	Fluid viscosity
t	Thickness of Plate

u	Injection Speed
T	Process Temperature
ρ	Melt Density
λ	Relaxation Time
k	Thermal Conductivity
Π	Dimensionless Number
u_i	Injection Speed
tanδ	Tangent of delta
n_{relax}	Relaxation Decay Constant
σ_{relax}	Maximum Relaxation Stress
μCT	Microcomputed Tomography
r	Pearson Correlation Coefficient
S	Percentage of Variation
R	Radius of Filament
δ	Melt film
W	Watt
N	Newton
%wt	Percent weight of loading
$\dot{\gamma}$	Shear rate
t	Time
s	Seconds
v_z	Velocity in the z-direction

List of Figures

1. Schematic of machine learning basic theory 9

2. Schematic explaining the theory of cross validation 10

3. Sigmoidal function logic theory 11

4. Desirability functions for different goals and how weights influence their respective shapes 12

5. A graphical depiction of a (a) 1-D hyperplane partition and a (b) 2-D hyperplane partitioning 13

6. An unclassifiable (a) 1-D problem transformed into a (b) 2-D problem via the Kernel Trick 14

7. Simple artificial neural network structure 15

8. An illustration of GPR and how more data increases the predictive capabilities. 16

9. Example of relaxation tests and its normalized version. 22

10. Images of samples processed at varying processing speeds with processing agent 26

11. Tests showcasing the increasing effect of processing agent on MFI. 26

12. Relaxation tests showing the decreasing effect of processing agent on λ. 27

13. Relaxation tests results showing the positive influence of comonomer content on λ 28

14. The confusion matrix of the optimized SVM classifier.. 30

15. The neural network architecture for test 1 after Bayesian optimization. 31

16. The neural network architecture for test 2 after Bayesian optimization. 32

17. The confusion matrix for test (left) 1 and (right) test 2. 33

18. The 10% and 30% relaxation tests showcasing their respective signal-to-noise ratios. 36

19. The method used to extract long-term material behavior from relaxation data 37

20. Workflow for the MATLAB program responsible for void analysis. 38

21. (a) μCT scan of a sample with 0% voids. (b) μCT scan of sample with 11.8% voids. (c) μCT scan of sample with 19% voids. (d) μCT scan of sample with 32.2% voids. 39

22. (a) An overlay of relaxation tests of blend 1 at varying levels of void content, and (b) the linear relationship between max stress experienced in relaxation testing and void content. 40

23. The relationship between voids and the rate at which stress decays for blend 9 (left) and 10 (right), characterized by n_relax. 40

24. The Pearson correlation coefficients for each parameter. 41

25. (a) The increasing relationship of void content on tan δ and (b) the influence of void content on hardness. 42

26. (a) The relaxation curves for blends 7, 8 and 9 while (b) represents the normalized curves. 43

27. (a) The relaxation curves for blends 1 and 4 while (b) represents the normalized curve, showing a large similarity in regard to the stress decay behavior. 43

28. Tests showing the influence of sulfur content and void content on tan δ for blends 7, 8 and 9. 44

29. The relationship between paraffin oil content and σ_relax of NR blend with 1.5 pph of sulfur. 45

30. Plot describing the similarity of unique blends by varying void content. 45

31. The influence of paraffin oil content on tan δ for a blend with 1.5 pph (a) and 2.5 pph of sulfur (b). 46

32. The Pareto Chart of Standardized Effects for (a) durometer reading and (b) σ_relax. 47

33. The Pareto Chart of Standardized Effects for (a) n_relax and (b) tan δ. 47

34. The curved response of sulfur content on n_relax, further confirming the results in the Pareto chart. 48

35. The parity plots for all four ANN models. 49

36. The results from the sensitivity analysis for both the linear regression baseline and the ANNs. 50

37. The parity plots describing Predicted vs. Experimental for GPR. 50

38. Graphical depiction of the 3D printing process via FFF 54

39. micro-CT scan of Nylon with short glass fiber reinforced 3D printed beads. 55

40. The melting experiment of applying rotation to the plastic rod while exerting a downward force onto a heated surface. 56

41. Small-scale experimental setup to prove the influence of viscous heating on melting behavior. 57

42. Pressure melt removal experiments of Nylon 66 at 280°C for varying rod diameters and rotational speeds.
43. Pressure melt removal experiments of Nylon 66 at 295°C for varying rod diameters and rotational speeds.
44. Pressure melt removal experiments for the Nylon 66 3.175 mm diameter case at varying temperatures and at two distinct forces.
45. (a) Pressure melt removal experimental results using PEEK with a 6.35 mm rod and (b) 4.7625 mm diameter rod
46. Pareto chart analysis of the input parameters for the PEEK melt throughput experiments.
47. Pareto chart analysis of the input parameters for the PA66 melt throughput experiments.
48. Schematic of the general construction of the modified extruder end used to provide extrusion length, force and temperature data during the 3D printing process [124].
49. Photo of the existing setup where the distinct key features are highlighted within the schematic (Indirect drive system, camera, load cell and nozzle)
50. (a) Overall cross-section of the design showing the static (blue) and rotating region (green). (b) Zoomed-in view of the region which shows the surface in which filament comes into contact with the rotating surface.
51. Raw experimental data points extracted from the instrumented 3D printer for tests at 260°C
52. All datapoints extracted from 0 RPM trials using the instrumented 3D printer to show the effect of temperature and filament speed on forces.
53. Contour plots displaying the effects of all input variables on the output response

54. Surface plots from the RSM model extracted from the viscous heating 3D printer extrusion trials.
55. Pareto chart for the Nylon 66 glass-fiber reinforced extrusion trials using the instrumented viscous heating 3D printer
56. Void analysis of two 3D printed components using the viscous heating 3D printer

57. Void analysis on all samples to describe the independence of rotational speed of the nozzle on the void content within 3D printed samples.
58. Visual representation of how the angle pair is used to describe the orientation of a single fiber per Advani and Tucker's orientation method.
59. Orientation tensor examples described graphically with two case scenarios.
60. Graphical depiction of the conventional FFF 3D printing process
61. Fiber orientation distribution for a 3D printed specimen with rotation of the nozzle disabled.
62. Orientation analysis of a 3D printed specimen with rotation of the nozzle enabled for the last 2-layers of printing.
63. The a_{11} orientation tensor for all 3D printed samples with the rotating nozzle enabled compared against the a_{11} orientation tensor of a 3D printed sample with a stationary nozzle.
64. (a) Fiber length at distinct print temperatures with rotation disabled, and (b) print trials at 260°C while varying rotational speed of the nozzle and print speed
65. Fiber attrition present in the viscous heating 3D printer at 5000 RPMs.
66. Cross-sectional image of the a two beads 3D printed with rotation of the nozzle disabled, clearly showing the alignment of fibers in the print direction.
67. The bead orientations for two testing scenarios where the left is classified as the 90° print and the right figure is the 0° print.
68. (a) three-dimensional image reconstruction of the sample produced with rotation of the nozzle disabled. (b) the sample produced with rotation of the nozzle enabled.
69. Fiber migration towards the adjacent bead occurring when rotation is activated.
70. Testing results for the 90° samples realized in accordance with ASTM D673.
71. Mechanical tests of all 3D printed components showing the positive effects on overall mechanical performance of 3D printed parts.
72. The processing window for the viscous heating 3D printer represented as a volume created from the RSM analysis.

List of Tables

1. The injection molding parameters kept constant for all trials on the Arburg 60T injection molding machine (Molded by Intertek, the Netherlands). 19

2. Parameters used for the dimensional analysis. 23

3. SVM and LR results depicting weights assigned to input parameters based on the influence. 25

4. Results showing that an increase in comonomer content results in the material's inability to deform 28

5. 8-fold cross-validation accuracy reached with partial input parameters. 29

6. Sensitivity analysis results 32

7. Materials employed within this study 34

8. Blend formulation DOE whereas each blend has 5 pph of Zinc Oxide, 1 pph of Stearic acid, 1 pph of TMTD and 8 pph of Sodium Bicarbonate. 35

9. μCT scanning parameters. 37

10. Results from the RSM analysis where each accuracy is shown, as well as the influential constants within the model 46

11. The predictive capabilities of the ANN and the overall architecture for each model. 48

12. Summary of the blends that were classified as the optimal blend based on target properties. 52

13. Design of experiments for the small-scale experimental study referred to as the pressure melt removal experiment. 55

14. Design of experiments for the extrusion trials using the viscous heating 3D printer.

15. Model summary of the RSM model which predicts extrusion forces within the instrumented viscous heating 3D printer

16. μCT scanning parameters.

Introduction

The ability of acquiring experimental data has become more economically feasible, and for that reason machine learning scientist positions have been recently created with more frequency. Machine learning scientists focus on acquisition of data, processing and in the implementation of these big data sets within data-driven modeling algorithms to provide predictions for industry. It is important to note that one does not necessarily have the ability to predict all types of events, ranging from sale projections to scientific projections relating to material behavior if one has a lot of data. A crucial aspect of these data-driven modeling implementation studies is in the proper selection of training parameters that one will extract from real experimental set ups or simulation. Users must be able to select the training parameters that are the most influential for the output, and the appropriate algorithm for the specific data set to ensure noise is reduced and convergence rate is maximized, respectively. Regarding polymer science and machine learning, a bridge between both disciplines needs to exist in order to acquire valuable data, and to minimize the amount of experimentation needed to train a robust algorithm.

Data-driven modeling has the ability, if implemented appropriately, to predict material behavior, polymer process performance, formulations, and to provide controls information for close-loop systems in charge of optimizing process performance based on real experimental data, to name a few. Implementing data-driven modeling, such as machine learning within the above-mentioned cases is crucial as the plastics industry highly depends on one's experience to minimize loss-time. For example, a custom polymer blend formulator is compensated heavily for their experience as their knowledge will be leveraged to ensure they understand the effects one additive may incur on

the overall blend and the interacting effects each additive has on one another. Before industry started proposing eco-friendly initiatives to reduce their carbon footprint, the formulator's priority was to purely optimize performance and to not prioritize sustainability. Now with industry embracing sustainable materials development, they now must maximize performance while also minimizing the inclusion of additives detrimental to the environment. Such duty to now optimize two variables has turned into an exceedingly complex task, as these effects may incur non-linear effects to performance. For that reason, machine learning is a valuable tool which with the appropriate training data, one could model and predict material behavior for large amounts of theoretical experiments without having to physically conduct the experiments.

The aim of this work is to enable polymer engineers to predict highly non-linear occurrences with the aid of data-driven modeling toolboxes by providing algorithms, varying in complexity, capable of reverse engineering current materials, predicting defects during polymer processing, and employing a predictive system within fused filament fabrication (FFF) 3D printing which informs users of ongoing defects during 3D printing.

1. Background

1.1 Modeling Approaches

Machine Learning (ML) is a computational method in which mimics human learning by combining statistics and optimization methods. Using such methods allows for algorithms to classify or predict very complex events, and to uncover valuable information regarding influential factors to those outcomes [1]. Key insights extracted from the algorithms serve as guides for decision-making within the application and further acquisition of data allows for continuous improvements, accelerating the optimization of the system [2]. There exist various types of machine learning algorithms, but most fall within the two types of categories: Supervised learning or unsupervised learning.

Supervised learning involves a predictive algorithm that uses data that has the outcomes defined for training purposes. As seen in the flow chart below (Figure 1), a portion of the data is set aside for testing purposes while the remainder of the data is used for training where the model continuously adjusts its rules (for example: weights and biases) until the error between the predicted and actual value is minimized [3]. Unsupervised learning uses machine learning algorithms to analyze and group unlabeled data. The algorithm is in charge of identifying patterns and establishing connections between data without a user to aid in this classification [3].

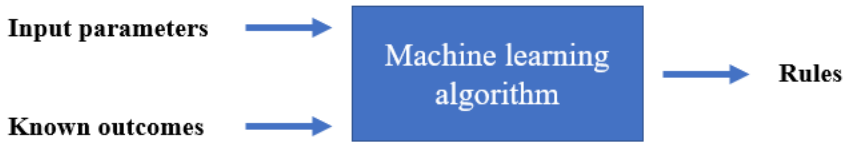

Figure 1. Schematic of machine learning basic theory

1.2 Best Practices for Machine Learning Algorithm Development

The excitement in industry with applying machine learning algorithms has led many to treat machine learning like a black box where one simply inputs large amounts of data into an artificial neural network (ANN) and calls it a day. A developer needs to choose the appropriate machine learning algorithm based on the size of the data, the desired outputs, and the type of inputs fed into the model. Once the testing algorithms are chosen, it is important to develop an unbiased training and testing strategy to ensure that underfitting and overfitting is avoided.

In general, overfitting is when a model has the ability to predict the training data too well. After training, it is unable to neglect noise and predicts inaccurate outputs. This occurrence can be avoided by not including data which has high variance and by introducing early stops within the model to ensure training is sufficient enough for prediction but not long enough in which the model learns from noise. Overfitting can also be avoided by implementing cross-validation (CV), which involves partitioning the data into n equal parts and conducting n independent trials where each part is used once for testing (Figure 2).

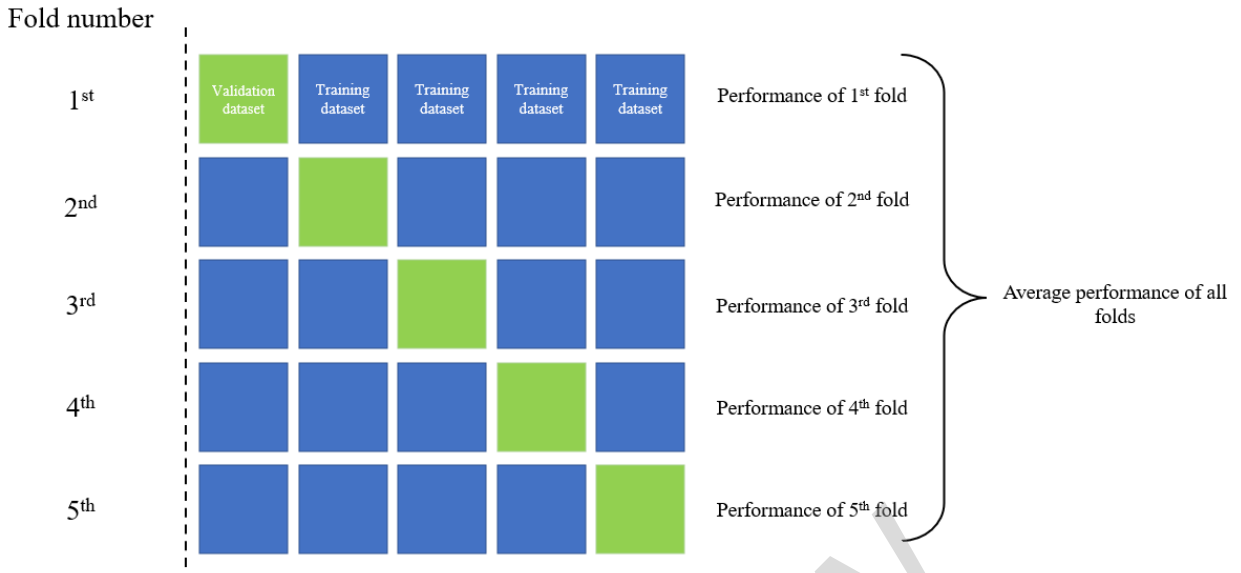

Figure 2. Schematic explaining the theory of cross validation

Underfitting arises when training does not converge and is not able to predict training data effectively. This issue may be addressed by increasing the model complexity, increasing the number of input parameters and by increasing the amount of data used in training to ensure it has enough information.

1.3 Linear and Logistics Regression

Linear regression is the simplest machine learning algorithm to implement as it involves finding a linear relationship between experimental data. Given an accurate model, this supervised machine learning model is primarily used to provide forecasting information based on user inputs and the parameters used for regression give insight into relationships between input and output variables [4]. Linear regression is described using the function seen in Equation 1 below, whereas the summation results in the weighted sum of its n features. Moreover, β_0 represents the intercept, β_i represents the feature weights, and ε corresponds to the difference between the computed prediction and the known outcome.

$$y = \beta_0 + \beta_1 x_1 + \beta_2 x_2 + \cdots + \beta_n x_n + \varepsilon \quad (1)$$

Logistics regression machine learning algorithms are primarily implemented in classification problems where the output can be described in binary format. In logistics regression, a weighted

sum of the inputs is passed through a sigmoidal activation function (Figure 3) whereas a 0 and 1 output is possible, ultimately allowing the user to represent a “No” with a zero and a “Yes” with the number one [5]. The classification model follows Equation 2 below and follows similar nomenclature to what is appreciated in Equation 1 above.

$$P(y=1) = \frac{1}{1+\exp\left(-(\beta_0 + \beta_1 x_1 + \beta_2 x_2 + \cdots + \beta_n x_n)\right)} \tag{2}$$

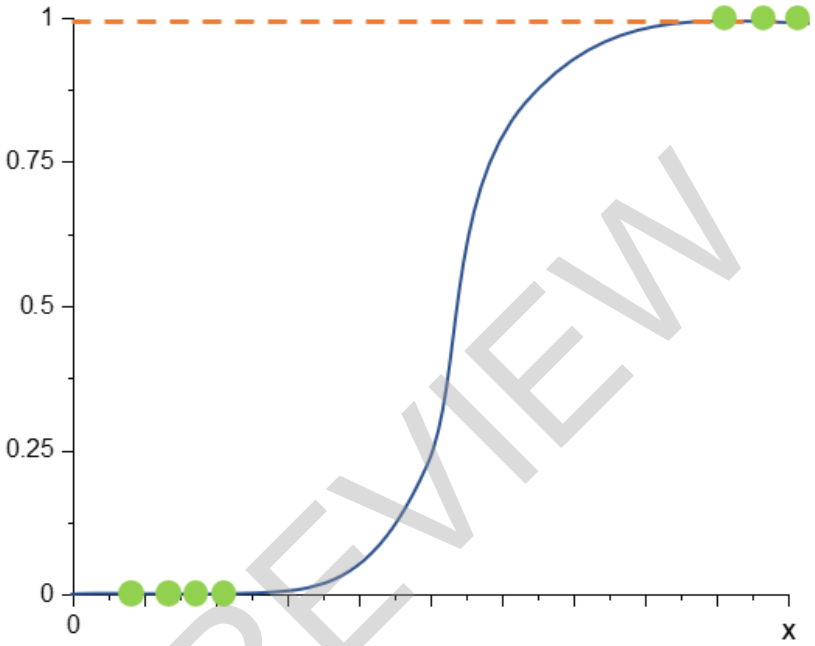

Figure 3. Sigmoidal function logic theory

Both Linear and Logistics regression models provide simple but resource-efficient predictive models which provide users with statistical information regarding significant input variables.

1.4 Response Surface Methodology

Introduced by George E. P. Box and K. B. Wilson in 1951, the Response Surface Method (RSM) uncovers the interconnectivity between various controllable factors and several response variables using nonlinear modeling. It should be acknowledged that RSM serves as an approximation method that provides a relatively simple method for modeling, estimating, and optimizing based on target parameters [6-8]. By use of mathematical and statistical techniques, an empirical model is created from experimental data and is used to evaluate the fit to a statistical model (linear, quadratic, cubic or two-factor Interaction), as described in Equation (3) below.

$$Y = a_0 + \underbrace{a_1A + a_2B + a_3C}_{\text{Linear}} + \underbrace{a_4A^2 + a_5B^2 + a_6C^2}_{\text{Quadratic}} + \underbrace{a_7AB + a_8AC + a_9BC}_{\text{Two-Factor}} \quad (3)$$

Using natural rubber formulation as an example, the independent variables A, B, and C may represent additives used within the formulation, such as: sulfur content, paraffin oil content, and void content, respectively. The output response Y represents the material property one aims to optimize. The coefficients ($a_0 - a_6$) determined by the model within the linear and quadratic sections dictate the influence each respective variable has on the output, Y, while the Two-Factor coefficients ($a_7 - a_9$) of the quadratic model above quantify the level of influence that interactions between two variables have on the output [6-9]. As mentioned above, formulating is a balance between various additives and RSM allows for the user to determine, to some degree, the interaction effects between two controllable variables.

Once the model is created, RSM allows for the optimization of a blend based on target responses, maximizing a specific response, or minimizing a specific response. The options available via RSM are of value as some additives may result in a dramatic increase in raw material expenditure, therefore, one can have a combination of various formulations which maximize certain controllable factors and minimize others to ensure cost rises are mitigated. Additionally, each target response may be given an importance value ranging from 0.1 to 10 if the user is more interested in some responses compared to others. If all target responses are of equal importance, then the default value should be 1. Moreover, if one target response is crucial for the user, the importance value can be increased up to a value of 10. Furthermore, weights may be assigned to each target response with values ranging from 0.1 to 10. The weights influence the desirability function shape between the lower/upper bounds and the target. Figure 4 below shows how different weights may influence the desirability function shape, where it can be seen that a larger weight creates a sharper, and quicker convergence to the target response.

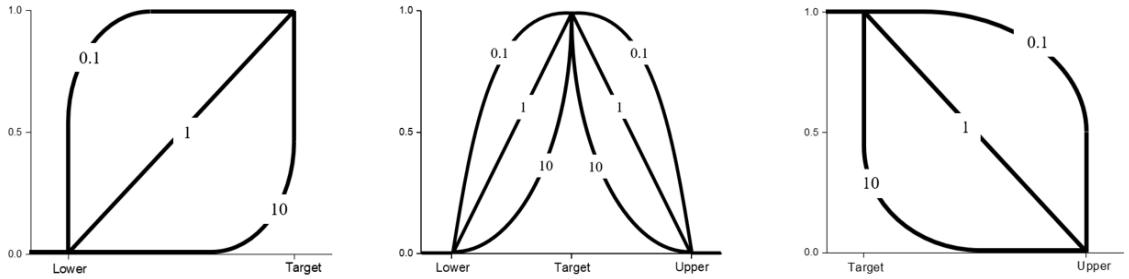

(**a**) (**b**) (**c**)

Figure 4. Desirability functions for different goals and how weights influence their respective shapes. (a) Minimize the response, (b) Achieve target value, and (c) Maximize the response

Although the quadratic function is mathematical, the statistical analysis of this regression model is key for interpreting the model. Minitab® 20 may be used for the RSM study whereas a 95% confidence level may be selected as the threshold for statistical significance. The Pareto chart of the Standardized Effects lists the standardized coefficients to understand which terms have the highest influence on each given response. By observing the magnitude of the standardized effect, the user can understand which controllable factors are the most influential and if a combination of controllable factors creates significant change to the output response. The dashed line within the Pareto chart indicates a significance level of $\alpha = 0.05$, therefore, anything to the right of the line suggests a term that is statistically significant to the response [6-8,10].

Additionally, the Coded Coefficients, such as the coefficients and *p*-value for each respective controllable factor allow the user to determine if a specific term is significant. If $p - \text{value} \leq \alpha$, the association is statistically significant, and if $p - \text{value} > \alpha$, the association is not statistically significant. Finally, the Model Summary is described by the standard deviation of the distance between fit values and input data values (S), the percentage of variation within the model response (R^2), the adjusted R^2 which is the variation in the response adjusted for the number of predictors in the model relative to the number of observations (R^2_{adjusted}), and the R^2 of the predictions which indicates how well the model predicts the removed observations ($R^2_{\text{predictions}}$). It is important to note that if $R^2_{\text{predictions}}$ is substantially less than R^2 then this may indicate that the model tends to overfit.

1.5 Support Vector Machine

Support vector machine (SVM) is a supervised machine learning algorithm best suited for classification and regression-type analyses. This method functions by partitioning data into clusters which separate outcomes from one another [11]. Figure 5.a and 5.b below show how 1-D and 2-D hyperplanes partition datasets effectively, allowing for accurate classification.

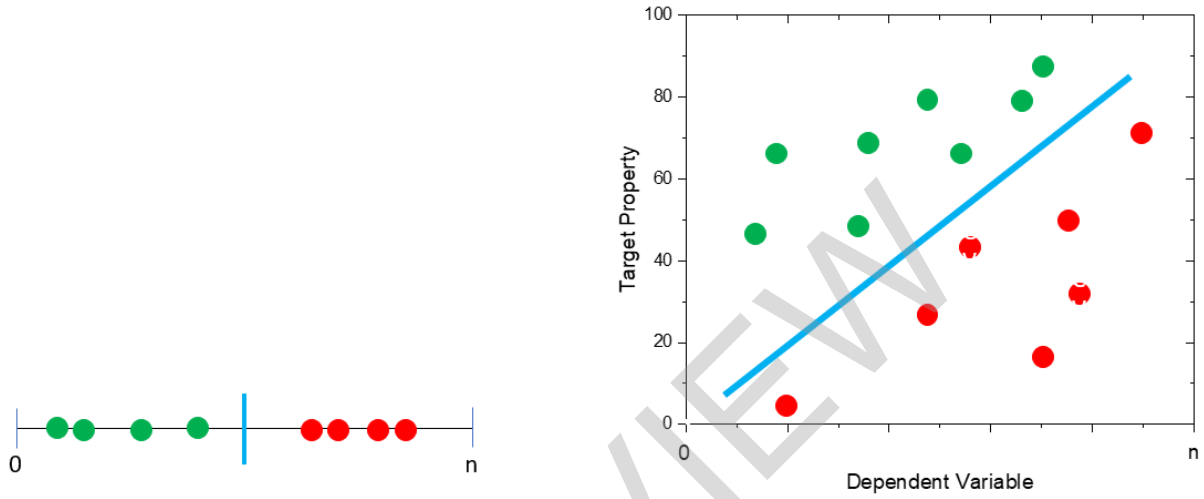

Figure 5. A graphical depiction of a (a) 1-D hyperplane partition and a (b) 2-D hyperplane partitioning

It allows for linear classification but is also capable of non-linear classification by introducing the "Kernel Trick", a method in which the input data is mapped onto a high-dimensional feature space [12], ultimately transforming the shape of the response curve. Figure 6.a and 6.b below shows a graphical representation of what the Kernel Trick can do when a dataset is deemed unclassifiable within a two-dimensional space. Figure 6.a shows scattered data within a 2-dimensional space which cannot be partitioned by a simple hyperplane. The algorithm will result in large amounts of misclassifications if the threshold is defined as a hyperplane. By using the polynomial Kernel trick, the shape of the data is altered and allows for a hyperplane to effectively partition the data within the three-dimensional space, as seen in Figure 6.b. The Kernel Trick is a valuable tool for polymer scientists formulating new materials as an additive does not always have an increasing/decreasing effect [13]. This is apparent for cases in which one assumes that increasing the amount of carbon-black (CB) reinforcement in a natural rubber (NR) formulation will result in an only increasing elongation at break, when evidently it is not the case as it has been proven that surpassing the 30

parts per hundred (pph) of natural rubber concentration begins to steadily decrease the elongation at break as the heavy load of reinforcement no longer has enough polymer material to adhere to, causing a weaker brittle fracture [14].

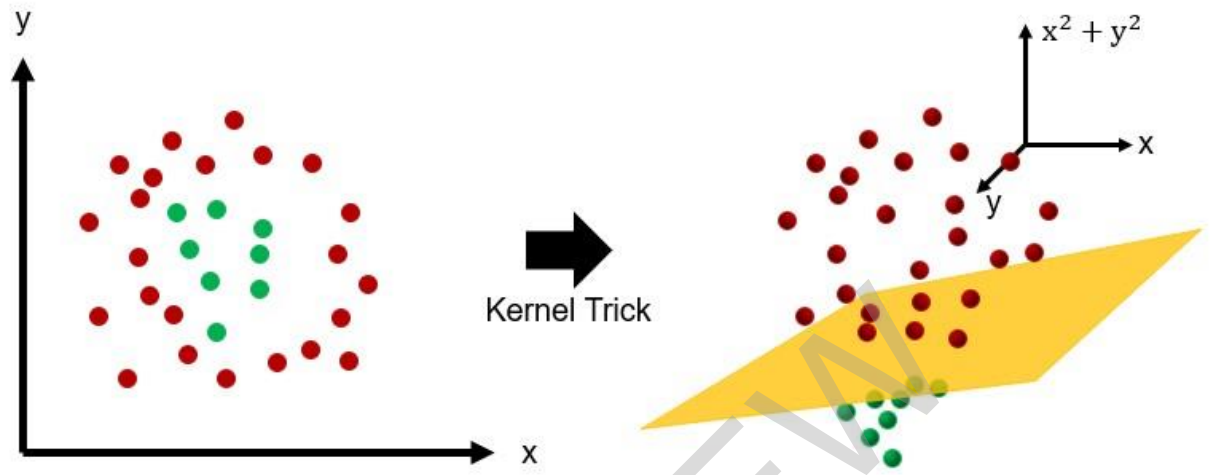

Figure 6. An unclassifiable (a) 2-D problem transformed into a (b) 3-D problem via the Kernel Trick

SVM is one of the most common types of machine learning algorithms implemented as it is effective with small datasets and can be implemented within higher dimensional spaces. The partitioning hyperplane follows the form of Equation 4 seen below, whereas alike linear regression, the weights and biases that make up the partition provide a quantitative insight into which input parameters have the most influence on the overall system.

$$y = \begin{bmatrix} w_1 \\ w_2 \\ \vdots \\ w_n \end{bmatrix} [x_1 \quad x_2 \quad \cdots \quad x_n] + b \tag{4}$$

$$x_i = \text{feature variable}$$

$$w_i = \text{feature weight}$$

$$b = \text{bias}$$